CRYSTAL GROWTH & DESIGN

pubs.acs.org/crystal

Article

Open Access

This article is licensed under CC-BY 4.0

Nucleation and Growth Kinetics in a Polymorphic System – The Case of Tolfenamic Acid

Peter T. Cardew,* Aurora J. Cruz-Cabeza, Roger J. Davey, Pietro Sacchi, and Thomas Vetter

Cite This: *Cryst. Growth Des.* 2026, 26, 7024–7036

Read Online

ACCESS | Metrics & More | Article Recommendations | Supporting Information

ABSTRACT: The control of crystallization processes in polymorphic systems remains a long-term goal at both laboratory and industrial scales. The rational design of processes that yield specific, desired crystal structures with suitable physical properties requires not only phase equilibrium data but also insights into the relative nucleation and growth rates of available crystal forms. For polymorphic systems that crystallize concomitantly, not only is such data largely unavailable, but also it is difficult to measure. This study determines the nucleation and growth kinetics of tolfenamic acid forms I and II from induction time distributions obtained from their crystallization in isopropanol in small volumes. The significant influence of crystal growth on both the form and analysis of induction time distributions has been examined, and methods to appropriately account for this effect are discussed. An analytical solution is developed, describing the induction time distribution in a dimorphic system in terms of the nucleation and growth kinetics of both forms. Despite the relevance of such data, this appears to be the first occasion in which such kinetic data have been obtained in a concomitantly crystallizing system.

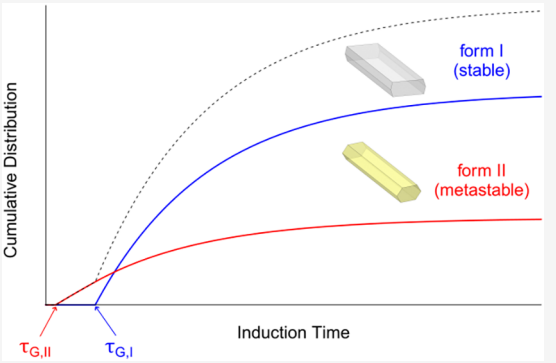

1. INTRODUCTION

The importance of crystalline polymorphs in the world of solid-state organic chemistry is well-known, arising largely from their differing crystal structures which impart differing physical properties. This phenomenon finds important relevance in the selection and development of pharmaceutical molecules, where both solubility and bioavailability are driven by crystal structure. This makes polymorph discovery, selection, and preparation important features of the overall research and development landscapes not only of pharmaceutical but also agrochemical and other specialty chemical products.[1]

In this paper, we return to the very fundamental question, first raised by Ostwald,[2] relating to crystallization processes in polymorphic systems namely, under a given set of experimental conditions, what controls the order in which polymorphs appear? It has been common practice in the past to associate the order of appearance of crystal forms with the relative magnitude of their nucleation rates, but this ignores the potential importance of crystal growth kinetics in the outcome of a crystallization experiment.[3] Consequently, in previous papers[4,5] we have defined and exemplified the use of the "Ostwald Ratio" as a way of constructing kinetic "phase diagrams" based on the temperature dependence of the growth and nucleation rates of the forms under consideration. This reveals that both are required for a full comprehension of the crystallizing system and for predicting experimental conditions likely to lead to the preparation of a desired polymorph. The limited availability of the requisite kinetic data, however, restricts the use of this concept. While growth rate data for individual polymorphic forms may be measured by direct macroscopic techniques,[6] access to nucleation kinetics is much more problematic, and little data exists.[6]

Previously, much use has been made of the stochastic nature of induction times when measured in small volumes as a way of accessing relevant kinetic data.[8] This is achieved by exploiting the fact that the overall nucleation rate decreases with decreasing volume such that nucleation time scales can become longer than growth time scales. Here, the measured times are assumed to reflect essentially the time required to create the first primary nucleus, but growth can be accounted for by taking the shortest induction time as the growth time. Secondary nucleation, leading to the shower of crystals that are finally detected, is considered to be a much faster process.[9] For systems in which only one crystal form exists, this has proved a successful means of accessing and quantifying nucleation rates.[8−11] For polymorphic systems able to crystallize concomitantly, Maggioni et al.[12] found that with no data on the nature of the polymorph nucleated, one can only determine an overall nucleation rate for the system—which is the sum of the individual polymorph rates. Their analysis

Received: May 6, 2026
Revised: July 14, 2026
Accepted: July 15, 2026
Published: August 10, 2026

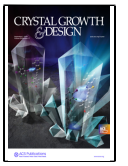

ACS Publications

© 2026 The Authors. Published by American Chemical Society

Downloaded from pubs.acs.org/cgdefu/article-pdf/26/17/7024/6647610/acs.cgd.6c00631.pdf by FACHHOCHSCHULE NORDWESTSCHWEIZ FHNW user on 04 September 2026

maintains the assumption that both forms grow sufficiently fast compared to the nucleation rates so that the distribution of observed induction times is equivalent to the distribution of nucleation times.

Our aim in this paper is to explore how this technique might be applied in a polymorphic system to enable the determination of the nucleation rates of *individual* polymorphs. A key question to be addressed is whether growth processes have a material impact on the distribution of induction times and, consequently, the determination of nucleation rates. In order to address this, both the theory and analysis have been extended to account for the possibilities that growth is not instantaneous and that growth times may depend on the polymorph crystallized.

As a suitable system for study, we have chosen the anti-inflammatory drug tolfenamic acid (TFA). The crystallization and solid-state chemistry of this molecule have been well explored with nine polymorphs known to date. Of interest here are the stable Forms I (TFA-I, white crystals) and metastable Form II (TFA-II, yellow crystals), which are easily crystallized from most organic solvents[13−19] and, through their color difference, easily distinguishable at the point of nucleation. Forms III to VIII, in contrast, have only been prepared by crystallization on templating agents, either in solution or by sublimation.[20−22] The most recently discovered Form IX, however, can also be grown from isopropanol (IPA) but only at low temperatures, as reported by Sacchi et al.[23] Here, therefore, we pursued further work on TFA Forms I and II in IPA and present new data for the cumulative induction time distributions of the two forms. Models relating these induction times to nucleation and growth rates of the forms are developed; the relative importance of crystal growth rates versus nucleation rates in this system is revealed; conclusions are drawn with respect to limitations of both the experimental technique and the models, and comments are made concerning the wider relevance of Ostwald's Rule which is used as a common heuristic.

2. MATERIALS AND METHODS

2.1. Materials

Tolfenamic acid (TFA) was purchased as the stable polymorph, Form I, from Fluorochem Ltd. Isopropyl alcohol (IPA) was purchased from both Fischer Scientific UK Ltd. and Honeywell Research Chemicals, according to its availability. Both were >98% pure.

2.2. Solubility of TFA and Supersaturation

The solubility of TFA in IPA was measured previously, and here, we used the values as reported in ref 13 (see SI1). At 25 °C, solubility values for the stable Form I (TFA-I) and the metastable Form II (TFA-II) are, respectively, 0.00393 mole fraction (0.0172 gTFA/gIPA) and 0.00430 mole fraction (0.0188 gTFA/gIPA). These values were then used to calculate the supersaturation ratios, S_i, for each polymorph in the solutions used in our experiments

$$S_i = \frac{x_i}{x_i^*} \tag{1}$$

where x_i and x_i^* are the actual and saturation mole fractions of each polymorph.

2.3. Measurement of Induction Times

Two Technobis Crystallization Systems (formerly Avantium Technologies) Crystal16 multivial reactors were used to measure the change in turbidity upon formation of a crystalline precipitate from supersaturated solutions. The use of the Crystal16 for measurement of induction times has been well documented.[10,24] Briefly, all crystallizations were performed in HPLC vials fitted with magnetic stirrer bars of the same shape and dimension for each sample vial. Each reactor holds 16 vials. Fresh stock solutions of TFA-I in IPA were prepared in the same way for each experiment. Weighed masses of TFA-I and IPA were mixed at about 45 °C to create solutions of the desired supersaturation ratio when cooled to 25 °C at various fixed rates. One ml aliquots of this hot stock solution were transferred to preweighed vials using a micropipette. The vials were immediately sealed and their weight checked to ensure equal distribution of solution between them. New clean vials were used in each case, except for two experiments, for which previously used vials were reused after cleaning with acetone. TFA is very soluble in acetone, thus making this solvent ideal for cleaning the glassware. The vials were sealed against evaporation using conventional screw-top polypropylene caps with PTFE septa screwed tightly. Vials were further weighed after the experimental cycle and data for vials with a mass variation larger than 0.05% were rejected.

Crystallization induction times (t_{ind}) were recorded as the difference between the time at which a vial reached the working temperature of 25 °C and the time at which the transmission of light (red light, peak wavelength 645 nm) in each vial started decreasing due to the formation of crystalline particles. At this point, the vial is said to have nucleated or crystallized—these terms are used interchangeably in this text. Bespoke Python3 scripts were written first to extract the time/turbidity data from the Crystal16 software but also to obtain the times at which the temperature was stable and equal to 25 °C (also accounting for instrument calibration) and the times at which the turbidity started decreasing (accounting for possible false positives due for example to the magnetic bar jumping around and interfering with the light beam or to changes due to lifting of the vial to check crystallized phase). The difference between these times gave the induction time.

The polymorph present at the time of crystallization was determined by periodically checking the Crystal16 to see (via the turbidity data) which vials had nucleated and then identifying the associated polymorph by the color of the crystals present. Thus, white crystals would indicate nucleation of TFA-I, bright yellow crystals nucleation of TFA-II, or shades of pale yellow a mixture of the two phases (see SI2, Figure S2.1 for typical images). In which case, it was assumed that the yellow form was first to appear. The consequences of relaxing this assumption are discussed on SI11, where the effects on the derived nucleation rates are shown to be minimal. This use of color as a means of phase identification was supported by PXRD[23] together with BRUKER DIFFRAC.Eva software. A database of simulated and experimental powder patterns, including those for mixtures of known compositions of Forms I and II and some collected at random from crystallized vials, was created. This was used to establish a relationship between the compositions of mixtures and their respective colors as observed visually. Since all visual observations were performed by a single researcher, a significant expertise was developed in recognizing mixtures of these tolfenamic acid polymorphs from their color. In this way, visual observation alone could give a good indication of the phase composition at the point of nucleation, and hence, it was possible to correlate the induction times with the related polymorph (or mixture). It is noted that the transformation of TFA-II to the stable TFA-I was found to be a solution-mediated process. In stirred and unstirred ambient conditions, pure TFA-II remained unchanged in IPA for several months. However, this time could be reduced to hours with the addition of TFA-I seed crystals and stirring. Also of note is the fact that the recently discovered polymorph of TFA, Form IX[23] was never observed (PXRD) in these experiments. Given that this new form takes ∼1 h to transform to TFA-II at 20 °C, it would have been revealed by pXRD. Its absence is thought to be because it requires rapid cooling of a solution saturated at 50 °C, suggesting that it needs much higher supersaturations than those available in the current study.

Nineteen experiments were run, numbered 1 to 19 in Tables 1 and 2. Here, we use the term "experiment" to refer to each set of multiple repeats performed in the Crystal16 under identical conditions of

Downloaded from pubs.acs.org/cgdefu/article-pdf/26/17/7024/6647761/0/acs.cgd.6c00631.pdf by FACHHOCHSCHULE NORDWESTSCHWEIZ FHNW user on 04 September 2026

https://doi.org/10.1021/acs.cgd.6c00631
Cryst. Growth Des. 2026, 26, 7024−7036

Table 1. Summary of the Induction Time Experiments Performed in This Work[a]

expt. no.	c (g/g)	T_{real} (°C)	S_I	S_{II}	method (temperature profile)	total number of repeats
1	0.0223	25.0	1.28	1.17	6.6 °C/min	276
2	0.0223	24.7	1.29	1.18	15 °C/min	176
3	0.0240	24.6	1.39	1.28	6.6 °C/min, hold at $T_{sat,I}$	208
4	0.0240	24.7	1.38	1.27	15 °C/min	196
5	0.0240	24.6	1.39	1.28	15 °C/min, hold at $T_{sat,I}$	160
6	0.0258	25.0	1.47	1.35	3 °C/min	196
7	0.0258	24.7	1.49	1.37	6.6 °C/min	198
8	0.0256	25.0	1.46	1.35	6.6 °C/min, hold at $T_{sat,I}$	216
9[b]	0.0258	24.8	1.48	1.36	15 °C/min	200
10	0.0256	24.9	1.47	1.35	15 °C/min	177
11[c]	0.0256	24.9	1.47	1.35	15 °C/min, 500 rpm	173
12	0.0273	25.0	1.56	1.43	6.6 °C/min, hold at $T_{sat,I}$	204
13[b]	0.0274	24.9	1.57	1.44	15 °C/min	157
14	0.0274	24.9	1.57	1.44	15 °C/min	216
15	0.0291	25.0	1.66	1.53	6.6 °C/min, hold at $T_{sat,I}$	204
16	0.0292	25.0	1.67	1.53	6.6 °C/min, hold at $T_{sat,I}$	203
17	0.0291	24.6	1.68	1.55	15 °C/min	198
18	0.0307	25.0	1.75	1.61	6.6 °C/min, hold at $T_{sat,I}$	195
19	0.0309	24.9	1.77	1.62	15 °C/min	197

[a]T_{real} is the average temperature of all four independent blocks of the Crystal16 according to the temperature calibration. Supersaturation ratios S_i for TFA-I and TFA-II were calculated according to this temperature value and using the respective solubilities of each phase. [b]Experiments were performed using cleaned, recycled vials rather than new ones. [c]The stirrer speed was 500 rpm. In the rest of the experiments, the stirrer speed was 900 rpm.

supersaturation, stirring, and cooling profile. Thus, the complete set of 19 experiments yielded a total of 3434 crystallization events. Table 1 summarizes both the conditions and the total number of repeats for each experiment. Thus, as illustrative examples from Table 1, we note that experiments, 2, 4, 9, 10, 13, 14, and 17 were run with a stirring rate of 900 rpm (chosen by comparison with previous work[8,10,24]) and a cooling rate (from 45 to 25 °C) of 15 °C/min, while experiments 1 and 7 used a stirring rate of 900 rpm with a slower cooling rate of 6.6 °C/min. In an extension of these conditions, experiments 3, 5, 8, 12, 15, and 16 also included a 4 min hold at the TFA-I saturation temperature corresponding to the composition used. This was included to minimize the cooling time spent supersaturated relative to TFA-I but undersaturated relative to TFA-II. In other experiments (using a cooling rate of 15 °C/min), both the effect of stirring rate (500 rpm was used in experiment 11) and cleaning of vials with acetone (in experiments 9 and 13) were briefly explored.[25,26]

Using two Crystal16 reactors meant that, for example, the 276 repeats of experiment 1 involved using each reactor about 8 times. This was achieved by cycling the reactors such that a single cycle of 16 vials was programmed to last either a maximum of 8 h or to be interrupted when all the vials had nucleated. After the completion of each cycle, the vials were reheated to 45 °C to dissolve all the crystallized solids and the process was repeated until at least 100 nucleation events were recorded. During each of these cycles, the vials were frequently inspected for the formation of crystals near the solution meniscus (crowning). At the beginning of each new cycle, any existing crowned solids were carefully redissolved by wetting them with the hot contents of the vial and manually rotating each vial.

3. MODELING AND ANALYSIS

3.1. Introduction

In this section, a series of models is developed for the cumulative distributions of induction times in a polymorphic system where the nucleation time scales are much longer than the growth time scales but are not necessarily negligible. It will be argued and shown that this growth time can be substantial in comparison to the stochastic nucleation time stemming from the formation of the first primary nucleation event and thus needs to be accounted for. The aim of developing these models is to achieve a better prediction of the nucleation kinetics from the analysis of the cumulative distribution of induction times. The starting point is a model for a system where the growth time scales are negligible compared to the nucleation time scales, which provides a useful reference case.

In 2011, Jiang and ter Horst[8] reported that the nucleation of crystals in small volumes follows a Poisson process due to the random nature of nucleation. This allows nucleation rates to be derived from measurement of the cumulative distribution of induction times, $Q(t)$, obtained from numerous experimental replicas. Provided growth time scales are very much smaller than the nucleation time scale, and under fixed conditions of supersaturation and temperature, the cumulative distribution of nucleation times, $P(t)$, in the vials is given by the exponential expression:

$$Q(t) = P(t) = 1 - \exp(-\Lambda_N t) \tag{2}$$

where Λ_N is a random variable characterizing the nucleation rate per vial. When the nucleation rate is considered volume dependent, the nucleation rate per unit volume, J_N, is given by Λ_N/V where V is the volume of solution in the vial. From eq 2, it follows that the average time it takes for a nucleation event to occur in each vial is

$$\tau_N = \frac{1}{\Lambda_N} \tag{3}$$

In 2017, Maggioni et al.[12] showed that eq 2 also applies to polymorphic systems with the same proviso that the induction times are determined solely by the nucleation process. For a polymorphic system, with several different crystal forms, π, each has its own nucleation rate, $\lambda_{N,\pi}$, and the cumulative probability distribution for a particular polymorphic form π is

$$Q_\pi(t) = P_\pi(t) = \frac{\lambda_{N,\pi}}{\Lambda_N}(1 - \exp(-\Lambda_N t)) \tag{4}$$

where the overall nucleation rate, Λ_N, is given by the sum of the individual polymorph nucleation rates

$$\Lambda_N = \sum_\pi \lambda_{N,\pi} \tag{5}$$

Equation 4 is an important result in that it shows that the shapes of the cumulative probability distributions for each of the forms are identical, are not totally independent, and differ only in the proportion of each form present

$$P_\pi(t) = \frac{\lambda_{N,\pi}}{\Lambda_N} P(t) \tag{6}$$

From eq 6, it follows that, at longer times, the proportion ξ_π of sample vials which nucleate with form π first is

Downloaded from pubs.acs.org/cgdefu/article-pdf/26/17/7024/6647761/0/acs.cgd.6c00631.pdf by FACHHOCHSCHULE NORDWESTSCHWEIZ FHNW user on 04 September 2026

https://doi.org/10.1021/acs.cgd.6c00631
Cryst. Growth Des. 2026, 26, 7024−7036

$$\lim_{t\to\infty} P_\pi(t) = \frac{\lambda_{N,\pi}}{\Lambda_N} \equiv \xi_\pi \tag{7}$$

Equations 2, 4, 6 provide the simplest characterization due to their minimal parameter requirements and will be referred to as Model A and serve as the baseline model for comparison with more complex alternatives.

A natural question to ask is what happens when the growth time is not negligible compared to the nucleation time scale. Jiang and ter Horst[8,9] took account of growth in a monomorphic system by noting that the induction time is the sum of the random nucleation time and the deterministic growth time, τ_G. In our model development, the growth time is assumed to be deterministic—an assumption that will be justified later in the manuscript. As a result, the cumulative distribution of induction times (CDIT), $Q(t)$, is related by a constant time difference to the cumulative distribution of nucleation times (CDNT) and hence

$$Q(t) = P(t - \tau_G) = 1 - \exp[-\Lambda_N(t - \tau_G)],\ t > \tau_G \tag{8}$$

They then equated this time delay τ_G, to the shortest measured induction time i.e., when the nucleation time is zero. By extension, it might be thought that for a polymorphic system, the cumulative distribution for the induction times is given by

$$Q_\pi(t) = P(t - \tau_{G,\pi}) = \xi_\pi(1 - \exp[-\Lambda_N(t - \tau_{G,\pi})]) \tag{9}$$

Equations 9 and 7 form the basis of Model B. However, this is only correct when the growth time scales of all the forms are the same (under fixed conditions like supersaturation, stirring rate, etc.). Although recognizing this limitation, Maggioni et al. used this approach for simplicity in their study of the trimorphic system of isonicotinamide in ethanol.[12]

In order to explore the impact of different growth times, consider a dimorphic system with a slow-growing stable form α and a fast-growing metastable form β. After nucleation of the α form, there is a time window $(\tau_{G,\alpha} - \tau_{G,\beta})$ when the faster-growing form β can nucleate and appear prior to the appearance of the slow-growing form. The probability for this to happen is given by

$$W = 1 - \exp[-\lambda_\beta(\tau_{G,\alpha} - \tau_{G,\beta})] \tag{10}$$

In this situation, a "natural" extension of eq 9 is

$$Q_\pi(t) = \tilde{\xi}_\pi(1 - \exp[-\Lambda_N(t - \tau_{G,\pi})]),\ t > \tau_{G,\pi} \tag{11}$$

where

$$\tilde{\xi}_\alpha = (1 - W)\xi_\alpha \tag{12}$$

$$\tilde{\xi}_\beta = \xi_\beta + W\xi_\alpha = W + (1 - W)\xi_\beta \tag{13}$$

$W\xi_\alpha$ is simply the proportion of vials in which the α form nucleated first, but Form β was seen at the point of detection. Equations 11, 12, 13 form the basis of Model C. While Model C does predict the long-term behavior correctly, it does not capture some of the behavior at early times. This can be seen by noting that for times less than $\tau_{G,\alpha}$ only the faster-growing β form can be present. During this early period, the cumulative distribution for the β form must follow the equation for a monomorphic system

$$Q_\beta(t) = 1 - \exp[-\lambda_\beta(t - \tau_{G,\beta})],\ t < \tau_{G,\alpha} \tag{14}$$

It follows that by the time the system reaches $\tau_{G,\alpha}$ crystals of the β form will have been observed in a fraction $Q_\beta(\tau_{G,\alpha})$ of the vials. From eq 14

$$Q_\beta(\tau_{G,\alpha}) = 1 - \exp[-\lambda_\beta(\tau_{G,\alpha} - \tau_{G,\beta})] = W \tag{15}$$

which by comparison with eq 10 is just W. It follows that, at this point in time, there are $(1-W)$ of the vials in which crystallization has not been observed. The appearance of crystals in these remaining vials follows that given by Model C. Thus, for the slow-growing form, we have

$$Q_\alpha(t) = (1 - W)\xi_\alpha(1 - \exp[-\Lambda_N(t - \tau_{G,\alpha})]),\ t > \tau_{G,\alpha} \tag{16}$$

and for the faster-growing β form

$$Q_\beta(t) = W + (1 - W)\xi_\beta(1 - \exp[-\Lambda_N(t - \tau_{G,\alpha})]),\ t > \tau_{G,\alpha} \tag{17}$$

The overall cumulative distribution function can be obtained by combining eqs 14, 16, 17 to give

$$Q(t) = \begin{cases} 0 & t < \tau_{G,\beta} \\ (1 - \exp[-\lambda_{N,\beta}(t - \tau_{G,\beta})]) & \tau_{G,\beta} < t < \tau_{G,\alpha} \\ W + (1 - W) & t > \tau_{G,\alpha} \\ \quad (1 - \exp[-\Lambda_N(t - \tau_{G,\alpha})]) & \end{cases} \tag{18}$$

Equations 14, 16, 17, 18 form the basis of Model D. It can be seen from eq 18 that the overall cumulative distribution function is no longer the simple exponential form but now involves two exponential expressions, which introduces a step-like feature into the distribution function for sufficiently different growth times of the two polymorphs.

In passing, it is noted that if $\tau_{G,\alpha} = \tau_{G,\beta}$ eq 18 simplifies to eq 8. However, this condition is likely to occur at most only at one supersaturation. Comparison of these models with simulations (see SI3.3 and 3.4) is given in the Supporting Information, where it is shown that while good agreement can be obtained for the overall cumulative distribution, $Q(t)$, there can be a substantial variance for the underlying distributions, $Q_\pi(t)$. Another aspect of the exact solution is that for the slow-growing form (eq 14), this has an exponential form, while for the fast-growing form, it is more complex (eqs 15,17). This is also the case for the overall nucleation rate (eq 18).

Following this analysis, two models will be applied here to investigate the concomitant crystallization kinetics of TFA-I and II:

Model A. This is a reference case and represents the simplest model to characterize the cumulative distribution function for the overall induction time. Growth time scales are assumed to be negligible when compared to those of the nucleation time scales. In this case, the cumulative distribution function of the induction times is identical to that for the nucleation times which are characterized by eq 2.

Model D: In this model, the growth time scales are treated as non-negligible and not the same. The growth time scales are estimated from the shortest times observed for crystals of a particular form to be detected in one of the vials. The cumulative distribution functions of the induction times for each form are determined by eqs 14-17.

Downloaded from pubs.acs.org/cgdefu/article-pdf/26/17/7024/6647761/0/acs.cgd.6c00631.pdf by FACHHOCHSCHULE NORDWESTSCHWEIZ FHNW user on 04 September 2026

https://doi.org/10.1021/acs.cgd.6c00631
Cryst. Growth Des. 2026, 26, 7024−7036

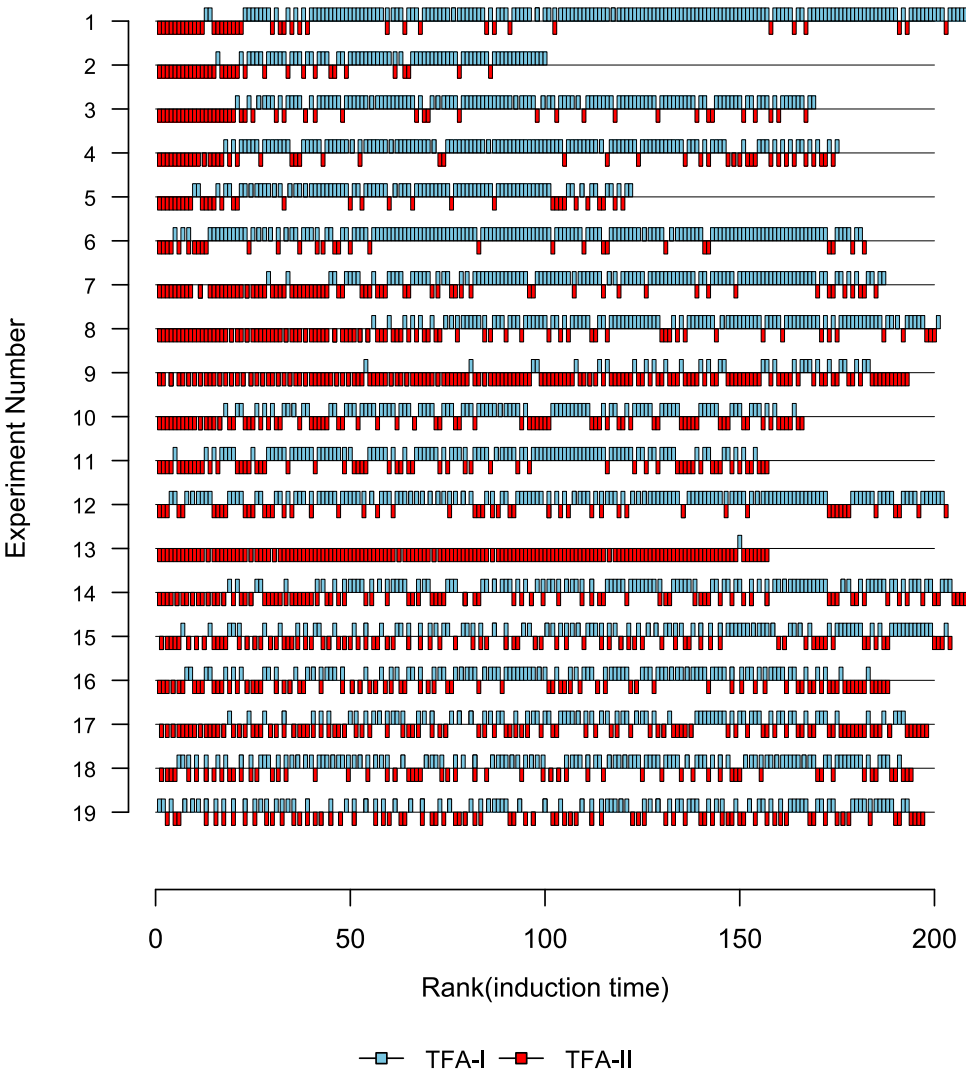

Figure 1. A rug plot showing how the ordered sequence in induction times varies for the two polymorphs. To enhance the differentiation between the boxes, they have been placed above and below the line according to their form for each experiment.

Further analyses of models A to D are given in the Supporting Information and include comparison with computer simulations.

3.2. Data Review

A summary of the results of the experiments undertaken are given in Table 2. For each set of experimental conditions (supersaturation, cooling rate etc.), the total number of independent crystallization experiments (i.e., number of vials used) is recorded together with their outcomes (TFA-I, TFA-II, no crystallization) and the number of vials in which crystallization occurred. These latter are then further divided depending on the initial polymorphic outcome of the sample. From these data, the percentage of samples relating to the occurrence of each form was calculated, and ξ_{II} was estimated from the fraction of sample vials in which form II appeared first. For example, for experimental series 1, 276 replicas were performed, of which 66 did not crystallize during the observation period. Of the remaining 210 repeats, 171 nucleated as TFA-I and 39 as TFA-II. Thus, of the total number of replicas (276), 76% crystallized, of which 62% led to TFA-I as the first appearing form and 14% to TFA-II. In this case, ξ_{II} is 0.18.

One way to review the experimental data is to display it as a multicolored rug plot (Figure 1). The location for each crystallization event in a time sequence can be determined by calculating the rank of the measured induction times. Each crystallization event can then be colored according to the form outcome. Thus, from Figure 1, it can be seen that the first event in all but one case is the appearance of the metastable TFA-II, even though in 16 out of 19 experiments most crystallization events were of the stable TFA-I (Table 2). Indeed, in many cases, the second and third events also resulted in TFA-II. Now, if growth were instantaneous, then the first few nucleation events would more likely have resulted in the stable form since as already mentioned the TFA-I was the dominant outcome in most experiments. The fact that the contrary is observed is evidence that the growth time scales are not negligible and that the primacy of the metastable form in most experiments can only be explained if it is faster growing than the stable form.

Experiments 9 and 13 stand out as being quite different from the others in that there is a significant increase in the proportion of vials containing TFA-II. In both experiments, all (experiment 13) or some (experiment 9) of the vials were reused from other prior experiments after cleaning. Experi-

Downloaded from pubs.acs.org/cgdefu/article-pdf/26/17/7024/6647610/acs.cgd.6c00631.pdf by FACHHOCHSCHULE NORDWESTSCHWEIZ FHNW user on 04 September 2026

https://doi.org/10.1021/acs.cgd.6c00631
Cryst. Growth Des. 2026, 26, 7024−7036

Table 2. Summary of Crystallization Outcomes for Each Experimental Series, Giving As Numbers and Fractions of Outcomes

		number of outcomes			percentage of outcomes			percentage crystallized polymorph ($\xi_{I \text{ or } II}$)	
expt. no.	total vial.	TFA-I (white)	TFA-II (yellow)	no cryst	TFA-I (white)	TFA-II (yellow)	no cryst	TFA-I (white)	TFA-II (yellow)
1	276	171	39	66	62.0	14.1	23.9	81.4	18.6
2	176	67	33	76	38.1	18.8	43.2	67.0	33.0
3	208	123	46	39	59.1	22.1	18.8	72.8	27.2
4	196	126	49	21	64.3	25.0	10.7	72.0	28.0
5	160	89	33	38	55.6	20.6	23.8	73.0	27.0
6	196	151	31	14	77.0	15.8	7.1	83.0	17.0
7	198	112	75	11	56.6	37.9	5.6	59.9	40.1
8	216	107	94	15	49.5	43.5	6.9	53.2	46.8
9	200	30	163	7	15.0	81.5	3.5	15.5	84.5
10	177	88	78	11	49.7	44.1	6.2	53.0	47.0
11	173	98	59	16	56.6	34.1	9.2	62.4	37.6
12	204	149	54	1	73.0	26.5	0.5	73.4	26.6
13	157	1	156	0	0.6	99.4	0.0	0.6	99.4
14	216	111	102	3	51.4	47.2	1.4	52.1	47.9
15	204	105	99	0	51.5	48.5	0.0	51.5	48.5
16	203	102	101	0	50.2	49.8	0.0	50.2	49.8
17	198	88	110	0	44.4	55.6	0.0	44.4	55.6
18	195	129	65	1	66.2	33.3	0.5	66.5	33.5
19	197	109	88	0	55.3	44.7	0.0	55.3	44.7

ments conducted with cleaned vials thus had substantially different polymorphic outcomes when compared to experiments conducted under the same conditions but with new, unused vials (see, e.g., Table 2, experiments 9 vs 10 and 13 vs 14).

Different cooling rates had some effect on the relative proportions of each polymorph, although it was difficult to identify any trend. The single run with a different stirring rate of 500 rpm (experiment 11) indicated that the stirring rate appeared to have some effect on the measured induction times (average time 8047 s, compared to 5714 s at 900 rpm as in experiment 10).

In 15 out of the 19 experiments, crystallization was not observed in some vials during the observation period (Table 2). This leads to right data censorship, and consideration into how this missing data is handled is required. In this analysis, the assumption is made that the disposition of the two forms in the censored data is the same as that in the uncensored data (for further details, see SI5).

3.3. Preliminary Data Analysis

For each experimental series, the cumulative distribution of induction times was plotted against the induction time (time when crystals were first detected in a sample vial), and then, the data were fitted to eq 2 (model A) to determine the overall nucleation rate using a nonlinear fitting routine (see SI6 for further details).

The results are summarized in Table 3. A selection of the data and associated fits to eq 2 is shown in Figure 2. It is noticeable that for the four lowest supersaturations, the curves have a sigmoidal form rather than the exponential form that eq 2 predicts. This further suggests that the assumption that the induction time is dominated by nucleation may not be valid.

In order to understand this behavior, the cumulative distribution of induction times for each form was plotted versus time. Figure 3 shows the results from experiments 1 and 8 (the rest in SI7, Figures S7.1, S7.2, and S7.3). As can be observed, the forms of the cumulative distributions of the two forms appear to be different. In particular, the time delays for

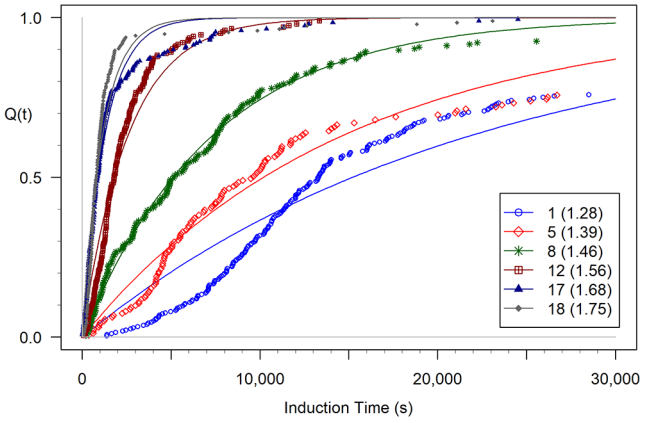

Figure 2. Cumulative distribution of induction times versus induction time for 6 experiments with various supersaturations (see legend), data fitted using eq 2 as per Model A.

the onset of crystallization of the two forms are quite different, confirming that growth of the crystals cannot be neglected and that the growth time scales for the two forms are substantially different.

The significance of this difference between the cumulative distributions was quantified by performing both the *t* and the Mann−Whitney tests. The power of a *t*-test is at a maximum when the underlying distribution is normal and declines as the distribution moves away from normality. A more powerful test in these situations is provided by the nonparametric Mann−Whitney test. Applying the *t*-test to the data from 18 experiments found there to be a significant difference at the 95% level of confidence in 7 cases (results from experiment 13 were excluded since there was only one event associated with the stable form). Applying the Mann−Whitney test, it was determined that in 13 out of 18 experiments the distribution for the two forms was significantly different at the 95% level of confidence (see SI4 and Table S4.1 for further details). The conclusion of this is that the hypothesis that the cumulative

Downloaded from pubs.acs.org/cgdefu/article-pdf/26/17/7024/6647610/acs.cgd.6c00631.pdf by FACHHOCHSCHULE NORDWESTSCHWEIZ FHNW user on 04 September 2026

https://doi.org/10.1021/acs.cgd.6c00631
Cryst. Growth Des. 2026, 26, 7024−7036

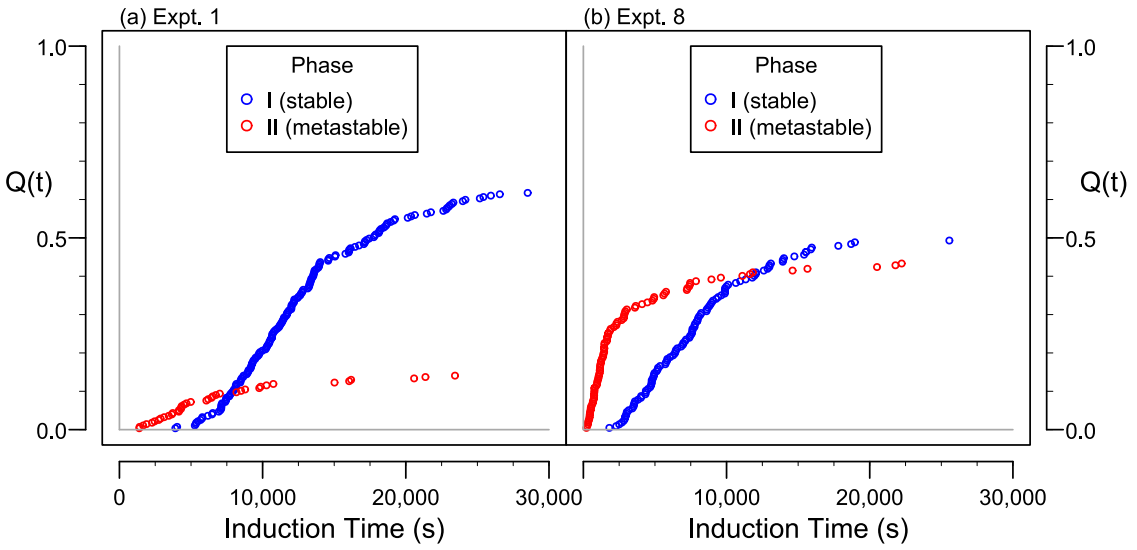

Figure 3. Cumulative distribution of induction times as a function of time in experiments 1 (a) and 8 (b).

Table 3. Nucleation Time Scales, τ_N Calculated for Models A and D[a]

expt no	model A	model D									
	τ_N	$\tau_{G,I}$	$\tau_{G,II}$	$\tau_{N,I}$		$\tau_{N,II}$		τ_N	W	RSE	
				value	se	value	se	value		initial	final
1	21926	3905	1385	19469	363	100128	11947	16299	0.025	0.081	0.045
2	36491	5330	1840	39762	887	64021	3472	24528	0.053	0.050	0.029
3	15917	2725	460	16363	234	44574	1627	11969	0.050	0.054	0.028
4	9912	1705	290	9758	195	33642	1751	7564	0.041	0.081	0.045
5	14694	1695	370	15744	319	46595	2669	11768	0.028	0.056	0.037
6	9258	860	265	10111	165	59662	5729	8646	0.010	0.050	0.041
7	5182	1070	130	6766	188	9390	333	3932	0.095	0.057	0.047
8	7352	1815	215	10215	402	10400	406	5153	0.143	0.073	0.061
9	3281	585	125	10504	861	2860	76	2248	0.149	0.082	0.065
10	7012	1060	335	10095	169	13115	243	5704	0.054	0.042	0.027
11	9556	1135	630	12264	207	23371	711	8043	0.021	0.050	0.034
12	2579	190	85	3270	49	9418	378	2427	0.011	0.041	0.038
13	3630		110			3466	17			0.021	0.017
14	1755	215	5	2870	45	3348	57	1545	0.061	0.035	0.029
15	1051	175	80	1676	35	1691	35	842	0.055	0.051	0.039
16	1186	155	25	1869	30	2273	38	1026	0.056	0.050	0.030
17	1266	205	5	2106	36	2148	31	1063	0.089	0.045	0.026
18	1136	165	90	1357	19	2978	81	932	0.025	0.052	0.032
19	727	85	110	1065	10	1245	16	574	−0.020	0.040	0.020

[a]Growth time scales used in model D are $\tau_{G,I}$ and $\tau_{G,II}$. *W* is given by eq 10. All time scales are in seconds. "se" is short for the standard error and "RSE" is the residual standard error.

distributions of the induction times for the two forms are the same must be rejected. We proffer that the most likely reason for this lies in the significant growth rate difference between the forms.

3.4. Accounting for Growth

In each experiment, the growth time scales of the two forms are taken to be the smallest value of the observed induction times for that form and are summarized in Table 3. These growth times are much smaller than the nucleation times but are not negligible. Table 3 shows that the overall nucleation time scale predicted by model D is 25% less than that in model A.

Figure 4 shows the resulting data and fits in four experiments (see SI7 for the full data set) for both forms based on model D. While the overall fit is good, for experiments 1 and 6, the coupling in eq 9 between the stable and metastable forms results in systematic deviations for the metastable TFA-II, suggesting that the nucleation time scale for TFA-II is shorter than that predicted.

In all experiments, the parameters ($\tau_{N,I}$, $\tau_{N,II}$) were found to be different with high statistical significance. It is noted that the nucleation rate for the stable TFA-I was nearly always greater than that of the metastable TFA-II. As seen in Table 3, there were four exceptions to this (experiments 8, 9, 15, and 17). Most notable was experiment 9 (in this experiment, some of the sample vials had been cleaned and reused), where the nucleation rate for TFA-II was more than four times that of the stable form. Comparing these data with those from experiment

https://doi.org/10.1021/acs.cgd.6c00631
Cryst. Growth Des. 2026, 26, 7024−7036

Downloaded from pubs.acs.org/cgdefu/article-pdf/26/17/7024/6647610/acs.cgd.6c00631.pdf by FACHHOCHSCHULE NORDWESTSCHWEIZ FHNW user on 04 September 2026

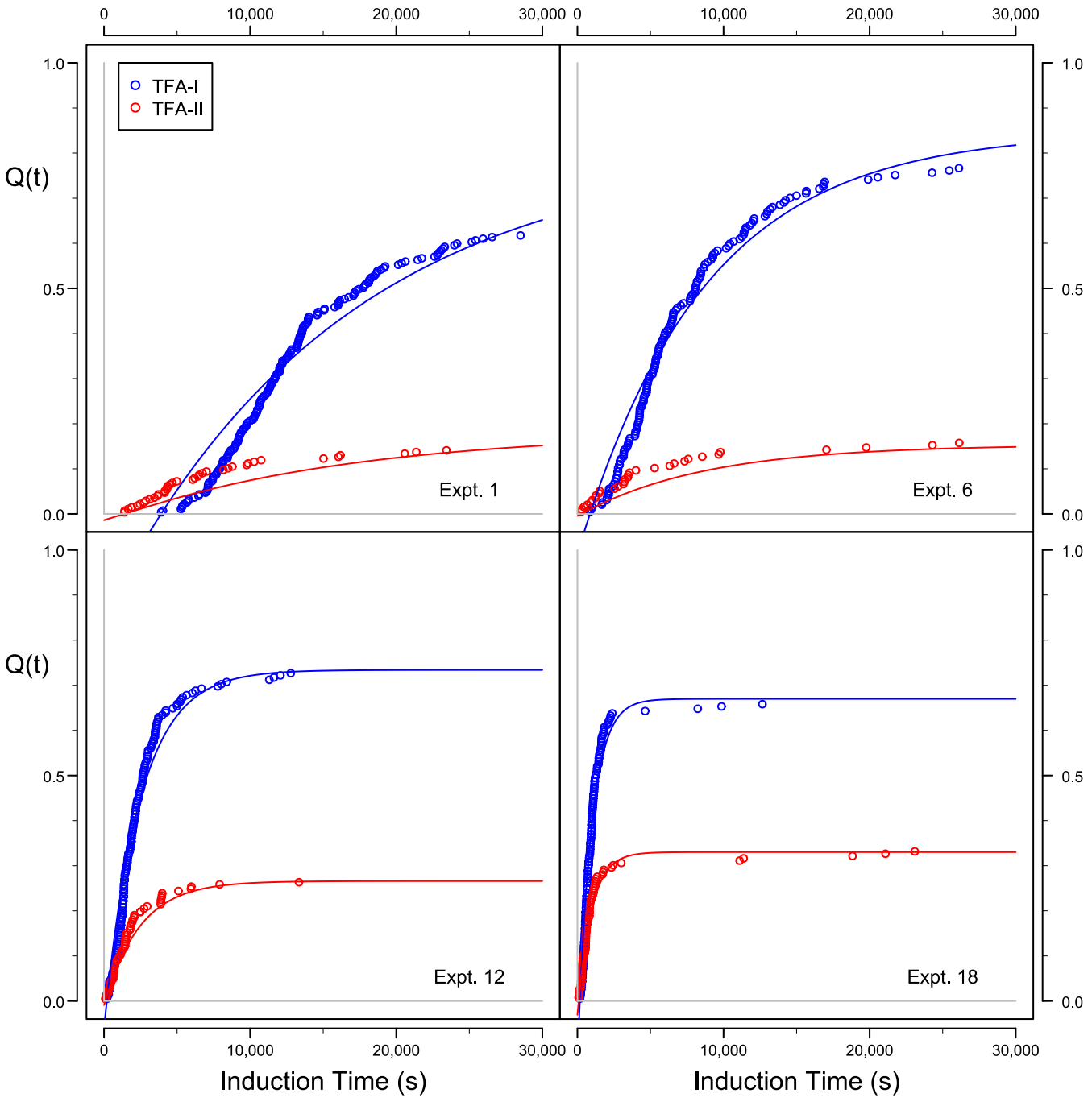

Figure 4. Graphs of the cumulative distribution of induction times versus induction time by form observed for four experiments and fitted curve using Model D.

10 (which was a repeat of 9 but with only new vials) showed that the major change was the nucleation rate of the metastable form. By comparison, the other three exceptions were all marginal in magnitude.

W is a measure of the probability of a metastable crystal being observed before the stable form is nucleated after that of the stable form. From Table 3, it is seen that *W* is less than 20% and, in most cases, less than 10%. In experiment 19, *W* has a negative value. This reflects the fact that the estimated growth time scale for the stable form is shorter than that of the metastable form. However, this difference is small (85 s against 110 s) and could be a statistical anomaly associated with the randomness of nucleation events. Full details of data fitting can be found in Section S8.

3.5. Crystallization Kinetics

3.5.1. Nucleation Rates. One of the purposes of these experiments is to gather information on the relative nucleation rates of the two forms (see SI9.1 for the full data set of numerical J values). A widely used expression (from classical nucleation theory, CNT) for the nucleation rate is[7]

$$J = \lambda/V = A S \exp\left(-\frac{B}{\ln^2 S}\right) \tag{19}$$

https://doi.org/10.1021/acs.cgd.6c00631
Cryst. Growth Des. 2026, 26, 7024−7036

Downloaded from pubs.acs.org/cgdefu/article-pdf/26/17/7024/6647761/0/acs.cgd.6c00631.pdf by FACHHOCHSCHULE NORDWESTSCHWEIZ FHNW user on 04 September 2026

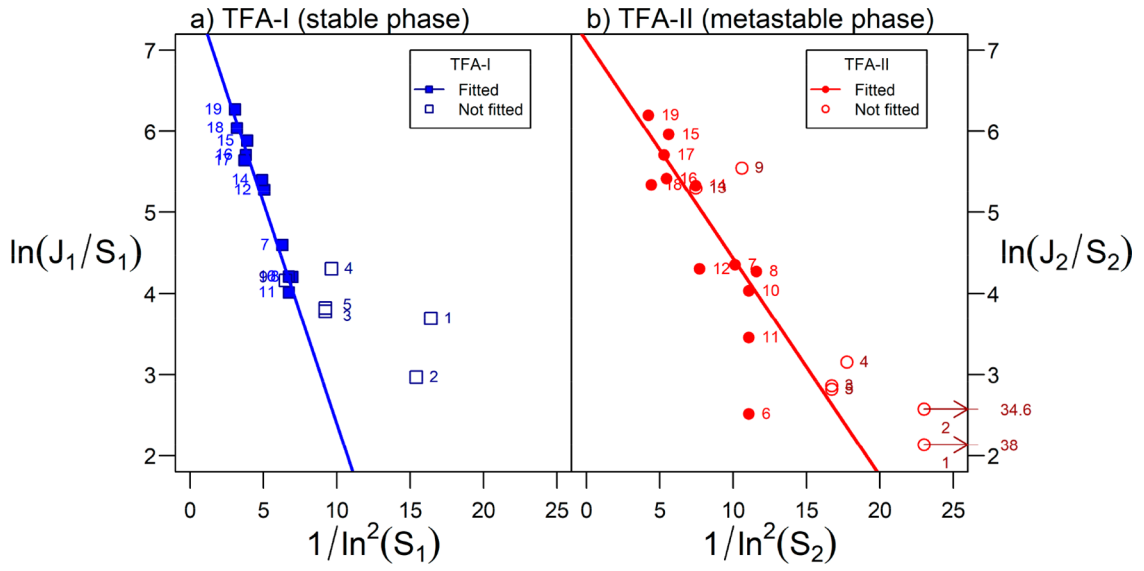

Figure 5. Plot of ln(J/S) versus $1/\ln^2(S)$ for (a) the stable form and (b) the metastable form (numbers refer to experiment number).

Table 4. Values and Statistical Significance of the Nucleation eq 20

	parameter A				parameter B				
form	A (m^{-3} s^{-1})	se	*p*-value	sig.[a]	B	se	*p*-value	sig.[a]	RSE
I	2304	422	0.000	***	0.51	0.05	0.000	***	56.6
II	1282	536	0.038	*	0.27	0.08	0.006	**	122.7

[a]Signif. codes: 0"***" 0.001"**" 0.01"*" 0.05.

where *S* is the supersaturation ratio, *A* is a kinetic constant, and *B* is a thermodynamic constant. Plotting $\ln(J/S)$ versus $1/\ln^2 S$ provides a useful plot since this would be expected to show a linear relationship

$$\ln(J/S) = \ln(A) - \frac{B}{\ln^2 S} \tag{20}$$

The data for the two forms are plotted according to eq 20 and shown in Figure 5. The nucleation parameters A and B were determined for each form by applying nonlinear regression to the data (Table 3) using eq 20 and are summarized in Table 4. See SI 9.1 for derived values of the interfacial tensions and comparison of A and B with other literature values. The analysis yielded a good fit for the stable form but for the metastable form the data points are more widely scattered around the calculated trend. Data from several experiments were not included in this fitting. Those at low supersaturation (experiments 1 to 5) were excluded since they showed large deviations from the expected (i.e., CNT) relationship, with rates much higher than predicted from the fitted equation. Data from experiments 9 and 13 were also excluded, as in these experiments, the sample vials were cleaned prior to use, and as already discussed, this led to major differences in nucleation behavior.

In the case of experiment 9, the nucleation rate of TFA-I appears close to the predicted value of the fitted data, but the value for the metastable TFA-II is substantially higher than expected. In experiment 13, the reverse is true with the TFA-II rate lying close to the prediction while TFA-I, which has an immeasurably low nucleation rate, shows a large deviation from the fitted line. In the case of experiment 11, where a low stirrer speed was used, the nucleation rate for the stable form is close to that expected, but for the metastable form, it appears reduced, perhaps indicating that stirrer speed is selectively influencing the secondary nucleation rate which produces the shower of crystals detected.

In Figure 6, the ratios of the nucleation rates of the two forms are plotted against supersaturation, showing that in most

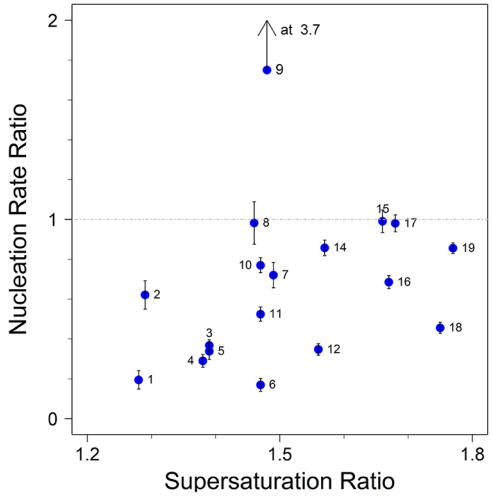

Figure 6. Plot of the ratio of nucleation rates (λ_{II}/λ_I) versus supersaturation ratio with respect to Form I.

cases this ratio is less than one, with the stable TFA-I being the faster nucleator. One exception is experiment 9, where the reverse is true and indicates that cleaning the sample vials dramatically impacted the nucleation rate of the stable TFA-I. This also applies to experiment 13, but since only one vial with the stable form was observed, the nucleation rate ratio could

https://doi.org/10.1021/acs.cgd.6c00631
Cryst. Growth Des. 2026, 26, 7024−7036

Downloaded from pubs.acs.org/cgdefu/article-pdf/26/17/7024/6647610/acs.cgd.6c00631.pdf by FACHHOCHSCHULE NORDWESTSCHWEIZ FHNW user on 04 September 2026

not be quantified but does indicate that it would be very large. The overall impression is that an unknown factor triggered by the cleaning procedure influences the nucleation of the stable TFA-I.

3.5.2. Growth Kinetics. The growth time is the time that has elapsed between the primary nucleation event and the detection of a decrease in optical transmission. During this period, the original nucleus grows, and additional nuclei may subsequently form through secondary nucleation. Indeed, visual inspection of the vials directly after nucleation was detected revealed the presence of thousands of small crystals, indicating that a substantial amount of secondary nucleation had occurred. The length of this time depends on instrument sensitivity and specific characteristics of the substance including crystal growth and secondary nucleation rates both of which will be polymorph dependent. In any particular experiment, the desupersaturation paths and hence the growth times might be expected to be similar for all vials. This is akin to assuming that the major source of stochasticity stems from the formation of the first nucleus via primary nucleation, with the random element associated with secondary nucleation being much faster than the primary. Indeed, the fact that models lumping these phenomena together as a "growth time" appear to fit the data well (as is the case in this work) is an indication that this assumption is justified.

To investigate how the growth times of both polymorphs vary across different experiments, the growth time for the metastable phase was plotted against that of the stable phase (Figure 7). This relationship provides insight into the comparative growth kinetics of the two forms. In particular, it shows that the growth times for the metastable polymorph are about one-third of those of the stable polymorph.

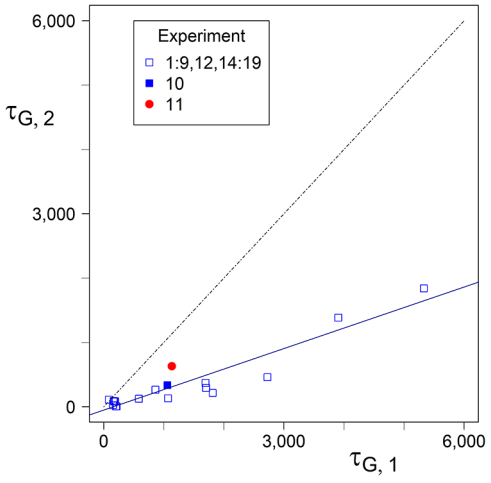

Figure 7. Plot of relative growth times of the metastable phase versus the stable phase. The filled-in square is experiment 10, and the red dot is experiment 11 which is a repeat of experiment 10 but at a lower stirrer speed (see Table 1), highlighting the degree to which stirrer speed has an influence on growth of the two polymorphs.

One interesting observation is the behavior of the growth times in experiments 10 and 11 (see Table 3). In experiment 10, the stirrer speed was 900 rpm, and the growth times of forms I and II were 1060 and 335s, respectively. Upon decreasing the stirrer speed to 500 rpm, these times increased to 1135 and 630 s. One interpretation of these data would be that the reduction in stirrer speed results in less crystal breakage and, hence, a lower rate of secondary nucleation, delaying the detection of crystals. The difference in growth times between the two forms would then be related to their individual mechanical properties.

Figure 8 shows the growth times for the two forms versus initial supersaturation. As expected, the growth times decrease

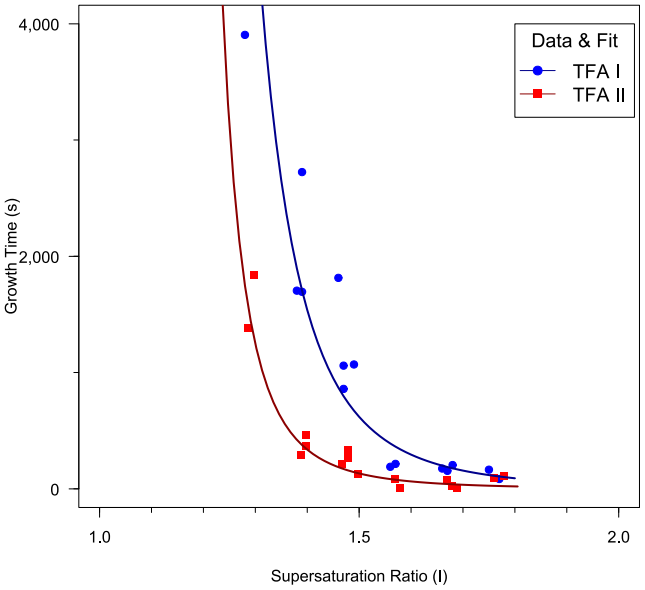

Figure 8. Plot of growth time versus supersaturation ratio for both polymorphs.

with increasing supersaturation. This is consistent with several of the mechanisms (growth and secondary nucleation) becoming faster at higher supersaturations. The data were fitted to a simple empirical power law expression viz

$$\tau_G = k_\tau (S - 1)^{-n} \quad (21)$$

In most experiments, the nucleation rate for the stable TFA-I is higher than that of the metastable TFA-II. However, in nearly all experiments, the vial with the earliest detection of a crystallization event yields TFA-II. The shorter growth times associated with TFA-II may explain why this occurs. However, in the end, it is the higher nucleation rate of the stable TFA-I that led to crystallization in most vials being triggered by the appearance of the stable TFA-I.

4. DISCUSSION

Although the measurement of CDITs in small volumes as a means of accessing nucleation rates has become relatively well-known in monomorphic systems, its use in concomitantly crystallizing polymorphic systems is more complex. There is, to our knowledge, only one other concomitantly crystallizing system, isonicotinamide, in which CDITs have been measured,[12] resulting in the estimation of the combined rate of nucleation of three polymorphs under the assumption of identical growth times of all forms. Consequently, the resulting model exhibited a familiar exponential probability distribution. Here, for the first time, we have been able to determine the individual CDITs of two polymorphs and show that they adopt a more sigmoidal shape than the pure exponential form observed in monotropic systems. A model has been developed that allows for differences in the growth time of the two forms and provides a good fit to the CDIT data. This model allowed

Downloaded from pubs.acs.org/cgdefu/article-pdf/26/17/7024/6647761/0/acs.cgd.6c00631.pdf by FACHHOCHSCHULE NORDWESTSCHWEIZ FHNW user on 04 September 2026

https://doi.org/10.1021/acs.cgd.6c00631
Cryst. Growth Des. 2026, 26, 7024−7036

the polymorph-specific nucleation rates to be extracted from our experiments. Additionally, the growth times for the two polymorphs are significantly different, behaving as expected with changes in experimental parameters.

Overall, the data show that the stable TFA-I nucleates faster than the metastable TFA-II (but they are quite close in magnitude). On the other hand, applying the nonparametric Mann−Whitney U-test found that the CDIT curves of the two forms were significantly different and that, in contrast to the relative nucleation rates, the growth time scale for the metastable TFA-II was much shorter than that of the stable form. While, as discussed in Section 3, this growth time includes components of both secondary nucleation and crystal growth, it is worth pointing out that the result is consistent with previous independent measurements of both single and overall crystal growth rates of the forms which confirm that TFA-II grows the faster[27,28] and discuss the underlying intermolecular interactions responsible.

Other points are worth mentioning. Adjusting the CDITs to account for the form-specific growth times produced a 25% reduction in the overall nucleation rate compared to values found if such effects had been neglected. Further, while in this paper, the growth time scales were estimated in the usual way from the shortest induction time of a particular form,[8,9] there are other potential methods. One way would be to calculate the growth time based on the top 25 and 75 percentiles of the individual CDITs of each polymorph (SI 6). Alternatively, the growth times can be included as additional parameters in the data fitting (eqs 14, 15, and 17). The disadvantage of the latter is that this doubles the number of parameters to be estimated, as well as presenting complex fitting issues. Using both these methods for our current data, it was found, for several cases, that the growth time scale for the metastable TFA-II was negative (SI 7). This suggests that, in these cases, nucleation occurred before the system reached the target temperature.

It is also worthwhile comparing our approach, in which the growth time incorporates multiple phenomena, with that of Maggioni and Mazzotti,[31] which models primary and secondary nucleation, growth, and dissolution separately. Apart from allowing simulation of the postnucleation evolution of a polymorphic system, they can also account for/predict the impact of operating parameters, such as the stirring rate or different ways of generating supersaturation over time. However, this additional insight comes at the expense of a larger number of kinetic parameters that are difficult to characterize from experimental data. Nonetheless, it is interesting to note that some of their model-based detection time distributions generated with assumed (but realistic) kinetic parameters (cf. Figure 4, right panel and Figure 6, bottom right panel in their work[31]) exhibit the sigmoidal shape found in our work, though our experimental data show this behavior to be more pronounced (cf. Figure 2 above).

In the context of our model system TFA, an interesting question is what proportion of the vials that initially nucleated in the stable form first were overtaken by the subsequent nucleation and growth of the metastable form. From eqs 12 and 13, the proportion of vials in which this occurs is $W\xi_1$. Figure 9 shows the results obtained for each experiment plotted against the supersaturation of Form I. The graph shows that in all experiments, the fraction of vials for which this occurred is less than 10%.

An assumption in these experiments is that the number of nucleation sites in each vial is the same and identical in terms

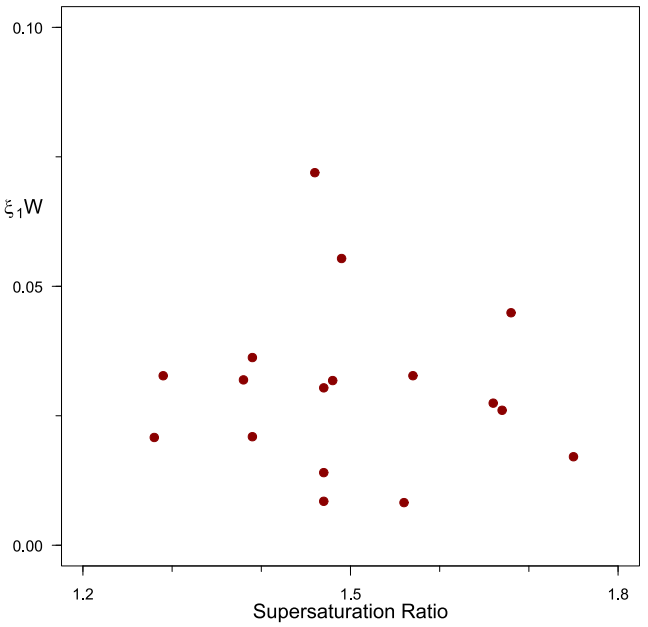

Figure 9. Plot of the proportion of vials in which the stable phase nucleated first but were overtaken by the faster-growing metastable phase ($\xi_1 W$) versus the supersaturation ratio of Form I.

of surface energy. While in large systems, these assumptions might be reasonable, for small volumes, there may be fewer nucleation sites, and their number may thus be variable among vials.[32] Indeed, inspection of the distribution curves shows some abrupt decreases in slope, which could reflect the absence of certain nucleation sites in some of the vials (see Figure 2). Studies of relevant monomorphic systems might lead to a better understanding of this matter. Another issue is whether the nucleation sites are present in the solution or on its surface. In experiments 9 and 13, where the sample vials were cleaned, there were (as discussed above) contradictory effects on the nucleation rates. While both have very low occurrences of TFA-I (see Table 2) in experiment 9, it is TFA-II that has a substantially higher nucleation rate than expected, while in experiment 13, TFA-I has a much lower rate than expected. This may indicate two opposing influences at work, resulting from cleaning with acetone. On the one hand, nucleation sites favoring TFA-I may have been removed by the solvent, while on the other, evaporation of acetone may leave imperceptibly small surface crystallites of TFA-II to catalyze its subsequent nucleation. This is certainly consistent with the observation that yellow crystals of TFA-II are often the result of evaporative crystallization from acetone at larger scales.

Another factor potentially influencing the outcome of these experiments is that supersaturation is generated by cooling solutions of fixed composition and hence is not instantaneous. For example, solutions designed to provide supersaturations of 1.3 and 1.8 at 25 °C first become supersaturated at higher temperatures as cooling proceeds (31 and 42 °C, respectively), leaving time (44 and 9 s, respectively) for nucleation to occur before the set temperature is reached. While these time scales are short when compared to those of the experiment, any nucleation or growth during this period could be exacerbated by the higher temperature, which would increase the rates of both processes (see SI10 for further discussion). This could help to explain some of the anomalous features of the

Downloaded from pubs.acs.org/cgdefu/article-pdf/26/17/7024/6647761/0/acs.cgd.6c00631.pdf by FACHHOCHSCHULE NORDWESTSCHWEIZ FHNW user on 04 September 2026

https://doi.org/10.1021/acs.cgd.6c00631
Cryst. Growth Des. 2026, 26, 7024−7036

cumulative distribution curve at the early stages of some of the experiments.

While a variety of experimental conditions were employed, the dependence of nucleation rate on supersaturation (in the range 1.28 to 1.77) was the most significant. The nucleation rate plots (Figure 5) of ln(J/S) versus $1/\ln^2(S)$ show that most of the data points lie on a straight line except those measured at low supersaturations (experiments 1 to 5), where the nucleation rate was much higher than expected for both forms but particularly for the metastable form. This is surprising and requires further investigation.

At this point, mention of Ostwald's Rule of Stages[2] seems appropriate since it has been the subject of much discussion and has been applied as a means of rationalizing the bulk outcome of crystallization experiments in polymorphic systems. Many workers[29] have interpreted their results in terms of the relative nucleation rates of various polymorphic forms and ignored possible growth effects. Most recently, Cardew and Davey[5,30] have demonstrated how the macroscopic manifestation of Ostwald's rule relies on both the relative nucleation and growth rates of the available forms. This current study, where we find that the faster nucleating polymorph is the stable form and also the slower grower, supports this conclusion and underlines the danger of attributing Ostwald's Rule and macroscopic crystallization outcomes solely to relative nucleation rates.

5. CONCLUSIONS

In this work, we have used the measured crystallization induction times to determine the nucleation and growth rates of two concomitantly crystallizing polymorphs of TFA. To our knowledge, this is the first example of such data. To aid our interpretation, a new analytical equation relating the cumulative distribution of induction times to the nucleation and growth times of polymorphs in a dimorphic system has been developed. Crucially, we have been able to show that in this case nucleation and growth act in opposite directions: the stable form, I, has the higher nucleation rate, while the metastable form, II, has the higher growth rate. Consequently, the first form to be detected is not necessarily the result of nucleation alone, and thus the potential role of crystal growth in determining the shape of the CDITs, and hence, the magnitude of the estimated nucleation rates has been explored in some detail.

From an academic perspective, it will now be possible, using our methodology, to explore the nucleation and growth of many more polymorphic systems and to fill a large and important gap in our knowledge of the associated kinetic processes. As shown in previous work,[5] the availability of such kinetic data enables the estimation of "kinetic" phase diagrams in which the appearance domains of various polymorphic forms can be elucidated. The availability of such information would clearly find significant application in process development where the isolation of specific polymorphs is required.

■ ASSOCIATED CONTENT

Supporting Information

The Supporting Information is available free of charge at https://pubs.acs.org/doi/10.1021/acs.cgd.6c00631.

Solubility data, photographs of reactors and crystals, full details of theory and simulation models, estimation of growth and nucleation time scales, induction times cumulative distributions, data fitting to various models, modeling of crystallization kinetics, methods for creating supersaturation, and analysis of crystallization experiments leading to mixed forms (PDF)

■ AUTHOR INFORMATION

Corresponding Author

Peter T. Cardew − *Department of Chemical Engineering, University of Manchester, Manchester M13 9PL, U.K.;* orcid.org/0000-0002-7829-7698; Email: peter.cardew@physics.org

Authors

Aurora J. Cruz-Cabeza − *Department of Chemical Engineering, University of Manchester, Manchester M13 9PL, U.K.; Department of Chemistry, Durham University, Durham DH1 3LE, U.K.;* orcid.org/0000-0002-0957-4823

Roger J. Davey − *Department of Chemical Engineering, University of Manchester, Manchester M13 9PL, U.K.;* orcid.org/0000-0002-4690-1774

Pietro Sacchi − *Department of Chemical Engineering, University of Manchester, Manchester M13 9PL, U.K.; The Cambridge Crystallographic Data Centre, Cambridge CB2 1EZ, U.K.;* orcid.org/0000-0001-5066-4508

Thomas Vetter − *Department of Chemical Engineering, University of Manchester, Manchester M13 9PL, U.K.; Institute of Pharma Technology and Biotechnology, FHNW University of Applied Sciences and Arts Northwestern Switzerland, Windisch, Aargau 5210, Switzerland;* orcid.org/0000-0002-4755-337X

Complete contact information is available at: https://pubs.acs.org/10.1021/acs.cgd.6c00631

Notes

The authors declare no competing financial interest.

■ ACKNOWLEDGMENTS

P.S. would like to thank Eli Lilly and Company for funding. The authors thank Dr. Susan M. Reutzel-Edens, President of SuRE Pharma Consulting, LLC, for helpful discussions.

■ NOMENCLATURE

CDIT	cumulative distribution of induction times
CDNT	cumulative distribution of nucleation times
SI	supporting information
RSS	residual sum of squares
RSE	residual standard error
se	standard error
$\lambda_{N,\pi}$	nucleation rate for phase π (s^{-1})
ξ_π	fraction of vials in which phase π is first observed first
τ_N	overall nucleation time scale (s)
$\tau_{N,\pi}$	nucleation time scale for phase π (s)
$\tau_{G,\pi}$	growth time scale for phase π (s)
π	phase index (1 or 2 in this case)
Λ_N	overall nucleation rate per vial (s^{-1})
A_π	nucleation parameter for phase π—see eq 11, (m^{-3} s^{-1})
B_π	nucleation parameter for phase π—see eq 11
G_π	relative growth rate of phase π
J	overall nucleation rate per unit volume (m^{-3} s^{-1})

Downloaded from pubs.acs.org/cgdefu/article-pdf/26/17/7024/6647610/acs.cgd.6c00631.pdf by FACHHOCHSCHULE NORDWESTSCHWEIZ FHNW user on 04 September 2026

https://doi.org/10.1021/acs.cgd.6c00631
Cryst. Growth Des. 2026, 26, 7024−7036

J_π	nucleation rate per unit volume for phase π (m^{-3} s^{-1})
N_{tot}	total number of samples converted
N_{Tot}	total number of samples in experiment
$P(t)$	cumulative distribution of nucleation' times
$P_\pi(t)$	partial cumulative distribution of nucleation times of phase π
$Q(t)$	cumulative distribution of induction times
$Q_\pi(t)$	partial cumulative distribution of induction times of phase π
S	supersaturation ratio (c/c_e)
S_π	supersaturation ratio for phase π, $c/c_{e,\pi}$
S_x	ratio of solubility of metastable phase to stable phase ($c_{e,II}/c_{e,I}$)
c	concentration (mol)
$c_{e,\pi}$	equilibrium concentration for phase π (mol)
t	time (s)

REFERENCES

(1) Bernstein, J. *Polymorphism in Molecular Crystals*; Oxford University Press, 2007 DOI: 10.1093/acprof:oso/9780199236565.001.0001.

(2) (a) Ostwald, W. Studien über die Bildung und Umwandlung fester Körper. 1. Abhandlung: Übersättigung und Überkaltung. *Z. Phys. Chem.* **1897**, *22*, 289−330. (b) Stranski, I. N.; Totomanow, D. Die Ostwaldsche Stufenregel. *Naturwissenschaften* **1932**, *20* (50), 905.

(3) Stranski, I.; Totomanow, D. Keimbildungsgeschwindigkeit und ostwaldsche stufenregel. *Z. Phys. Chem.* **1933**, *163A*, 399−408.

(4) Black, J. F. B.; Cardew, P. T.; Cruz-Cabeza, A. J.; Davey, R. J.; Gilks, S. E.; Sullivan, R. A. Crystal nucleation and growth in a polymorphic system: Ostwald's Rule, p-aminobenzoic acid and nucleation transition states. *CrystEngComm* **2018**, *20* (6), 768−776.

(5) Cardew, P. T.; Davey, R. J. The Ostwald Ratio, Kinetic Phase Diagrams, and Polymorph Maps. *Cryst. Growth Des.* **2019**, *19* (10), 5798−5810.

(6) Liu, Y.; Gabriele, B.; Davey, R. J.; Cruz-Cabeza, A. J. Concerning Elusive Crystal Forms: The Case of Paracetamol. *J. Am. Chem. Soc.* **2020**, *142* (14), 6682−6689.

(7) Davey, R. J.; Schroeder, S. L. M.; ter Horst, J. H. Nucleation of Organic Crystals—A Molecular Perspective. *Angew. Chem., Int. Ed.* **2013**, *52* (8), 2166−2179.

(8) Jiang, S.; ter Horst, J. H. Crystal Nucleation Rates from Probability Distributions of Induction Times. *Cryst. Growth Des.* **2011**, *11* (1), 256−261.

(9) Brandel, C.; ter Horst, J. H. Measuring induction times and crystal nucleation rates. *Faraday Discuss.* **2015**, *179* (0), 199−214.

(10) Sullivan, R. A.; Davey, R. J.; Sadiq, G.; Dent, G.; Back, K. R.; ter Horst, J. H.; Toroz, D.; Hammond, R. B. Revealing the Roles of Desolvation and Molecular Self-Assembly in Crystal Nucleation from Solution: Benzoic and p-Aminobenzoic Acids. *Cryst. Growth Des.* **2014**, *14* (5), 2689−2696.

(11) Cruz-Cabeza, A. J.; Davey, R. J.; Sachithananthan, S. S.; Smith, R.; Tang, S. K.; Vetter, T.; Xiao, Y. Aromatic stacking − a key step in nucleation. *Chem. Commun.* **2017**, *53* (56), 7905−7908.

(12) Maggioni, G. M.; Bezinge, L.; Mazzotti, M. Stochastic Nucleation of Polymorphs: Experimental Evidence and Mathematical Modeling. *Cryst. Growth Des.* **2017**, *17* (12), 6703−6711.

(13) Du, W.; Cruz-Cabeza, A. J.; Woutersen, S.; Davey, R. J.; Yin, Q. Can the study of self-assembly in solution lead to a good model for the nucleation pathway? The case of tolfenamic acid. *Chem. Sci.* **2015**, *6*, 3515−3524.

(14) Andersen, K. V.; Larsen, S.; Alhede, B.; Gelting, N.; Buchardt, O. Characterization of two polymorphic forms of tolfenamic acid, N-(2-methyl-3-chlorophenyl)anthranilic acid: their crystal structures and relative stabilities. *J. Chem. Soc., Perkin Trans. 2* **1989**, No. 10, 1443−1447.

(15) Blade, H.; Blundell, C. D.; Vitorica-Yrezabal, I. J. Crystal structures of tolfenamic acid polymorphic forms I and II with precise hydrogen-atom positions for nuclear magnetic resonance studies. *Acta Crystallogr., Sect. E:Crystallogr. Commun.* **2020**, *76*, 1421−1426.

(16) Mattei, A.; Li, T. Polymorph Formation and Nucleation Mechanism of Tolfenamic Acid in Solution: An Investigation of Pre-nucleation Solute Association. *Pharm. Res.* **2012**, *29* (2), 460−470.

(17) Mattei, A.; Mei, X.; Miller, A.-F.; Li, T. Two Major Pre-Nucleation Species that are Conformationally Distinct and in Equilibrium of Self-Association. *Cryst. Growth Des.* **2013**, *13* (8), 3303−3307.

(18) Abramov, Y. A.; Zhang, P.; Zeng, Q.; Yang, M.; Liu, Y.; Sekharan, S. Computational Insights into Kinetic Hindrance Affecting Crystallization of Stable Forms of Active Pharmaceutical Ingredients. *Cryst. Growth Des.* **2020**, *20* (3), 1512−1525.

(19) Tang, W.; Sima, A. D.; Gong, J.; Wang, J.; Li, T. Kinetic Difference between Concomitant Polymorphism and Solvent-Mediated Phase Transformation: A Case of Tolfenamic Acid. *Cryst. Growth Des.* **2020**, *20* (3), 1779−1788.

(20) López-Mejías, V.; Kampf, J. W.; Matzger, A. J. Polymer-induced heteronucleation of tolfenamic acid: structural investigation of a pentamorph. *J. Am. Chem. Soc.* **2009**, *131* (13), 4554−4555.

(21) Case, D. H.; Srirambhatla, V. K.; Guo, R.; Watson, R. E.; Price, L. S.; Polyzois, H.; Cockcroft, J. K.; Florence, A. J.; Tocher, D. A.; Price, S. L. Successful Computationally Directed Templating of Metastable Pharmaceutical Polymorphs. *Cryst. Growth Des.* **2018**, *18* (9), 5322−5331.

(22) Ranjan, S.; Devarapalli, R.; Kundu, S.; Saha, S.; Deolka, S.; Vangala, V. R.; Reddy, C. M. Isomorphism: 'molecular similarity to crystal structure similarity' in multicomponent forms of analgesic drugs tolfenamic and mefenamic acid. *IUCrJ* **2020**, *7* (2), 173−183.

(23) Sacchi, P.; Reutzel-Edens, S. M.; Cruz-Cabeza, A. J. The unexpected discovery of the ninth polymorph of tolfenamic acid. *CrystEngComm* **2021**, *23*, 3636.

(24) Xiao, Y.; Tang, S. K.; Hao, H.; Davey, R. J.; Vetter, T. Quantifying the Inherent Uncertainty Associated with Nucleation Rates Estimated from Induction Time Data Measured in Small Volumes. *Cryst. Growth Des.* **2017**, *17* (5), 2852−2863.

(25) Elzhov, T. V.; Mullen, K. M.; Spiess, A.-N.; Bolker, B. R Interface to the Levenberg-Marquardt Nonlinear Least-Squares Algorithm Found in MINPACK, Plus Support for Bounds. 2023.

(26) Davey, R. J.; Garside, J. *From Molecules to Crystallizers: An Introduction to Crystallization*; Oxford University Press, 2000 DOI: 10.1093/hesc/9780198504894.001.0001.

(27) Sacchi, P.; Neoptolemou, P.; Davey, R. J.; Reutzel-Edens, S.; Cruz-Cabeza, A. J. Do metastable polymorphs always grow faster? Measuring and comparing growth kinetics of three polymorphs of tolfenamic acid. *Chem. Sci.* **2023**, *14* (42), 11775−11789.

(28) Liu, Y.; Ma, C. Y.; Gong, J.; Roberts, K. J. Crystal Morphology and Associated Face-Specific Growth Kinetics of Tolfenamic Acid as a Function of Its Solution Crystallization Environment. *Cryst. Growth Des.* **2025**, *25* (21), 9322−9332.

(29) Cruz-Cabeza, A. J.; Taylor, E.; Sugden, I. J.; Bowskill, D. H.; Wright, S. E.; Abdullahi, H.; Tulegenov, D.; Sadiq, G.; Davey, R. J. Can solvated intermediates inform us about nucleation pathways? The case of β-pABA. *CrystEngComm* **2020**, *22* (43), 7447−7459.

(30) Cardew, P. T. Ostwald Rule of Stages−Myth or Reality? *Cryst. Growth Des.* **2023**, *23* (6), 3958−3969.

(31) Maggioni, G. M.; Mazzotti, M. A Stochastic Population Balance Equation Model for Nucleation and Growth of Crystals with Multiple Polymorphs. *Cryst. Growth Des.* **2019**, *19* (8), 4698−4709.

(32) Deck, L.-T.; Mazzotti, M. Characterizing and measuring the ice nucleation kinetics of aqueous solutions in vials. *Chem. Eng. Sci.* **2023**, *272*, No. 118531.

Downloaded from pubs.acs.org/cgdefu/article-pdf/26/17/7024/6647610/acs.cgd.6c00631.pdf by FACHHOCHSCHULE NORDWESTSCHWEIZ FHNW user on 04 September 2026

https://doi.org/10.1021/acs.cgd.6c00631
Cryst. Growth Des. 2026, 26, 7024−7036